Astron. Astrophys. 329, 559–570 (1998)

ASTRONOMY
AND
ASTROPHYSICS

Fine mesh calculations of dwarf nova outbursts

K. Ludwig and F. Meyer

Max-Planck-Institut für Astrophysik, Karl-Schwarzschild-Strasse 1, D-85748 Garching, Germany

Received 30 June 1997 / Accepted 4 August 1997

Abstract. We present new results from fine mesh calculations of dwarf nova outbursts. The vertical thermal and the radial viscous evolution of the accretion disk is followed simultaneously. This is essential for determining formation, structure, and propagation of transition fronts which are a fundamental constituent of the dwarf nova cycle. In addition to the equation of continuity of mass flow and the energy equation, we have solved the Navier-Stokes equations for the radial and the azimuthal velocity. This allows us to follow deviations of the azimuthal velocity from the Keplerian value. Results show, that these deviations are largest inside heating waves, but have only marginal influence on the outburst behavior. More important are the effects of lateral heat diffusion which cause an enlargement of the radial width of a heating wave. This leads to essential changes in the long-term evolution of the accretion disk. We compare our new results with earlier results (Ludwig et al. 1994), where we used the localized front approximation (Meyer 1984) and with results of fine mesh calculations of Mineshige (1987) and Cannizzo (1993).

Key words: accretion, accretion disk – cataclysmic variables – instabilities – stars: individual: VW Hydri

1. Introduction

Dwarf novae are a subclass of cataclysmic variables, i.e. close binaries consisting of a white dwarf primary and a low-mass main-sequence secondary which fills its critical Roche volume. The secondary loses mass through the inner Lagrangian point which then is accreted via an accretion disk by the primary. The defining characteristic of dwarf novae is that phases of low luminosity (quiescence) alternate with phases of high luminosity (outburst) in a semi-regular way. The outbursts which have amplitudes of 2-6 mag in the visual light occur at intervals of a few weeks or months, the maximum brightness lasting a few days to 20 days. There are also exceptions from this typical outburst behavior. For example, the dwarf nova system U Gem, where outbursts typically last 12 days, in October 1985 underwent an optical outburst of 45 days, duration unprecedented in the $\approx$ 100 yr that the star has been monitored (Mason et al. 1988).

We have investigated outbursts in dwarf nova accretion disks in the framework of the disk instability model. In this model the outburst phenomenon is explained as a cyclic change of the disk structure between a hot and a cool state. Transition waves, which separate a hot bright region from a cool dark region, propagate through the disk and initiate the light variation.

In this paper we perform high resolution calculations that include several effects left out before. We compare our results with those from previous calculations (Ludwig et al. 1994) which used the localized front approximation (Meyer 1984) and with fine mesh calculations by Mineshige (1987) and Cannizzo (1993). Here one has to note, that the results of most previous calculations seriously suffer from too coarse a resolution (see Cannizzo 1993). In particular, then the amount of lateral heat diffusion in the region of a transition wave is inevitably underestimated (see Mineshige 1987). Finally, our calculations allow us to investigate the influence of deviations of the azimuthal velocity from the Keplerian value on the outburst behavior. For this, in addition to the equation of continuity of mass flow and the energy equation we solve the Navier-Stokes equations for the radial flow and the azimuthal velocity. The deviation from the Kepler velocity is mainly produced by pressure forces. Inside transition fronts a steep gradient of the pressure occurs. Here deviations from the Keplerian flow can have an influence on the structure of the front, which may cause changes in the outburst behavior.

The method of our calculation is given in Sect. 2. Results are shown in Sect. 3 followed by a discussion in Sect. 4. A comparison of our results with those of Mineshige (1987), Cannizzo (1993) and Ludwig et al. (1994) is carried out in Sect. 5, and conclusions are given in Sect. 6.

2. Method of numerical calculations

We consider a geometrically thin and axi-symmetric disk. This assumption allows a separate treatment of the vertical (local) and radial (global) structure of the disk. This standard procedure to calculate a time-dependent disk is described in e.g. Ichikawa & Osaki (1992).

Send offprint requests to: F. Meyer

2.1. Basic equations for the radial structure

The basic equations governing the radial (global) structure for vertically integrated quantities in a disk are the equation of continuity, the Navier-Stokes equations for the radial flow velocity v_r and the azimuthal velocity v_φ, and the energy equation (see e.g. Bird et al. 1966). Though in thin disks the deviations from Kepler rotation are always very small their gradients in the steep transition fronts become of the same order as the gradients of the Kepler rotation themselves. They thus affect the frictional heating and angular momentum transport within the fronts. The evolution of such non-Keplerian disks is investigated here for the first time. In the vertically integrated form we use the vertically integrated quantities surface density Σ, pressure $\tilde{P}$, $r\varphi$-component of the viscous stress tensor $\tilde{\tau}_{r\varphi}$ and the midplane values temperature T and mean molecular weight μ. This is a generally used approximation (see Mineshige & Osaki 1983, Cannizzo 1993).

The equation of continuity is

$$\frac{\partial \Sigma}{\partial t} + \frac{1}{r}\frac{\partial}{\partial r}(r v_r \Sigma) = 0\,, \tag{1}$$

with r distance from the white dwarf.

The Navier-Stokes equation for the azimuthal velocity is

$$\frac{\partial p_j}{\partial t} + \frac{1}{r}\frac{\partial}{\partial r}(r v_r p_j) = -\frac{1}{r}\frac{\partial}{\partial r}(r^2 \tilde{\tau}_{r\varphi})\,, \tag{2}$$

with $p_j = r v_\varphi \Sigma$, the angular momentum per unit area,

$$\tilde{\tau}_{r\varphi} = -r f \frac{\partial \Omega}{\partial r} \tag{3}$$

the viscous stress tensor, where f denotes the viscosity integral (see Eq. 13) and Ω the angular velocity.

The Navier-Stokes equation for the radial flow velocity is

$$\frac{\partial p_r}{\partial t} + \frac{1}{r}\frac{\partial}{\partial r}(r v_r p_r) = \Sigma\frac{v_\varphi^2}{r} + \Sigma g_r - \frac{\partial \tilde{P}}{\partial r} - \frac{1}{r}\frac{\partial}{\partial r}(r\tilde{\tau}_{rr}) + \frac{\tilde{\tau}_{\varphi\varphi}}{r}\,, \tag{4}$$

where $p_r = v_r \Sigma$ is the momentum per unit area in radial direction and

$$g_r = -\frac{G M_{\rm WD}}{r^2} \tag{5}$$

the gravitational acceleration in radial direction, with G the gravitational constant, $M_{\rm WD}$ the mass of the white dwarf, and

$$\tilde{P} = \frac{\Re}{\mu}\Sigma T + 2H\frac{a}{3}T^4 \tag{6}$$

the pressure ($\Re$ gas constant, a radiation density constant). H is the isothermal scale-height

$$H = (\frac{\Re}{\mu}T)^{1/2}/\Omega_{\rm K}\,, \tag{7}$$

with $\Omega_{\rm K}$ the Keplerian angular velocity.

The vertically integrated components of the viscous stress tensor are given by (compare Ichikawa & Osaki 1994)

$$\tilde{\tau}_{rr} = -f\left(2\frac{\partial v_r}{\partial r} - \frac{2}{3r}\frac{\partial}{\partial r}(r v_r)\right) + \zeta\left(\frac{1}{r}\frac{\partial}{\partial r}(r v_r)\right)\,, \tag{8}$$

$$\tilde{\tau}_{\varphi\varphi} = -f\left(2\frac{v_r}{r} - \frac{2}{3r}\frac{\partial}{\partial r}(r v_r)\right) + \zeta\left(\frac{1}{r}\frac{\partial}{\partial r}(r v_r)\right)\,, \tag{9}$$

where ζ is the vertically integrated bulk viscosity. Here we take $\zeta = 0$ and note that terms of the same form are already included in the equations. It would not be appropriate to choose $\zeta = -\frac{2}{3}f$ as is sometimes done in physical literature in other contexts since here lateral compression involves vertical expansion and therefore (shear) viscosity.

The energy equation is

$$\begin{aligned} C_{\rm V}\left[\frac{\partial}{\partial t}(\Sigma T) + \frac{1}{r}\frac{\partial}{\partial r}(r v_r \Sigma T)\right] &= -2HT\left(\frac{\partial P}{\partial T}\right)_\rho \frac{1}{r}\frac{\partial}{\partial r}(r v_r) \\ -2\sigma T_{\rm eff}^4(T,\Sigma,r,M_{\rm WD},\mu) &- \tilde{\tau}_{r\varphi}\, r\frac{\partial \Omega}{\partial r} - \tilde{\tau}_{rr}\frac{\partial v_r}{\partial r} - \tilde{\tau}_{\varphi\varphi}\frac{v_r}{r} \\ +\frac{1}{r}\frac{\partial}{\partial r}\left\{r 2H\frac{4acT^3}{3\kappa\rho}\frac{\partial T}{\partial r}\right\} &+ \frac{1}{r}\frac{\partial}{\partial r}\left\{r 3 C_{\rm V}\Sigma\nu\frac{\partial T}{\partial r}\right\}\,. \end{aligned} \tag{10}$$

The specific heat at constant volume $C_{\rm V}$, the Rosseland mean opacity κ, $\left(\frac{\partial P}{\partial T}\right)_\rho$ and the kinematic viscosity ν are mid-plane values. The relation $\Sigma = 2\rho H$ is used to determine the density ρ at the mid-plane.

For the terms at the right hand side of the energy equation we proceed as follows. The relation between the effective temperature and the mid-plane temperature, the radiative cooling term $\sigma T_{\rm eff}^4(T,\Sigma,r,M_{\rm WD},\mu)$, is obtained from integration of the vertical structure as described in Sect. 2.2. For the viscous heating we have also considered, besides the "standard" $\tau_{r\varphi}$-heating term, the τ_{rr}- and $\tau_{\varphi\varphi}$-contributions. The last two terms in the energy equation represent the radial energy flux carried by radiative and by viscous processes (compare Taam & Lin 1984, Mineshige 1987, Cannizzo 1993). For optically thin regions, the radiative transport in radial direction is neglected.

In addition to the 4 basic equations we need a description of the viscosity. Godon(1995) has shown, how the standard alpha viscosity prescription (Shakura & Sunyaev 1973, Novikov & Thorne 1973) has to be modified if the rotation law of the disk is not Keplerian. For our calculations we used the parametrisation of the viscosity given by Godon:

$$\nu = \frac{2}{3}\alpha c_{\rm s} H \frac{|\partial\Omega/\partial r|}{|\partial\Omega_{\rm K}/\partial r|}\left(\frac{\bar{H}}{H}\right)^2\,, \tag{11}$$

where α is the viscosity parameter, $c_{\rm s}$ the sound velocity, and

$$\bar{H} = \frac{H}{1 + (r/H)|1 - \Omega^2/\Omega_{\rm K}^2|}\,. \tag{12}$$

For $\Omega = \Omega_{\rm K}$ this reduces to the standard Shakura-Sunyaev description. For the viscosity integral f we make use of a one-zone model for the vertical structure:

$$f = \int_{-\infty}^{+\infty} \nu\rho dz = \bar{\nu}\Sigma\,, \tag{13}$$

where $\bar{\nu}$ is taken as the value of ν in the mid-plane. With $c_s = \left(\frac{\partial P}{\partial \rho}\right)_T^{1/2} = (\frac{\Re}{\mu}T)^{1/2}$ and Eq. (11) we obtain:

$$f = \frac{2\alpha \Re T \Sigma}{3\mu\Omega_K} \frac{|\partial\Omega/\partial r|}{|\partial\Omega_K/\partial r|} \left(\frac{\bar{H}}{H}\right)^2 . \quad (14)$$

We take the two-alpha description, in order to fit observed light curves (see Sect. 2.3).

2.2. The approximation of the cooling function

To solve the system of differential equations the vertically integrated quantities have to be expressed as functions of Σ and T at each distance r. This involves a relation between $T_{\rm eff}$ and T (mid-plane), $\sigma T_{\rm eff}^4(T, \Sigma, r, M_{\rm WD}, \mu)$. Detailed results for vertical disk structure are given in Ludwig et al. (1994). The S-shaped thermal equilibrium curve consits of the hot branch (ionized matter), an intermediate branch (partial ionization) and a cool branch (unionized matter), optically thick or thin (compare Meyer-Hofmeister & Ritter 1992). For our calculations we use partly results of Ludwig et al. (1994) and partly, for simplicity, relations optained by Ichikawa & Osaki (1992), who consider only an optically thin cool branch, and by Cannizzo (1993).

2.2.1. The hot branch

We use the relations from Cannizzo (1993):

$$T = 8039\,{\rm K}\ {M_{\rm WD,1}}^{1/7}\, r_{10}^{-3/7}\, \alpha_{\rm h,0.2}^{1/7}\, \Sigma^{3/7}\, \mu_{0.6}^{-1/14} \quad (15)$$

and

$$T_{\rm eff} = 2414\,{\rm K}\ {M_{\rm WD,1}}^{9/56}\, r_{10}^{-27/56}\, \alpha_{\rm h,0.2}^{2/7}\, \Sigma^{5/14}\, \mu_{0.6}^{-15/56}, \quad (16)$$

where $M_{\rm WD,1} = M_{\rm WD}/\,M_\odot$, $r_{10} = r/10^{10}$ cm, $\alpha_{\rm h,0.2} = \alpha_{\rm hot}/0.2$ and $\mu_{0.6} = \mu/0.6$.

The relation for the effective temperature $T_{\rm eff}(T, \Sigma, r, M_{\rm WD}, \mu)$ is obtained by eliminating α by means of Eq.15 from Eq.16,

$$T_{\rm eff} = 37346\,{\rm K}\ {M_{\rm WD,1}}^{-1/8}\, r_{10}^{3/8}\, T_5^2\, {\Sigma_2}^{-1/2}\, \mu_{0.6}^{-1/8}, \quad (17)$$

where $T_5 = T/10^5$ K and $\Sigma_2 = \Sigma/10^2 {\rm g\,cm^{-2}}$.

2.2.2. The unstable intermediate branch

Suffix A and B denote values at the transition from the hot branch to the unstable branch and that from the unstable branch to the cool optically thick branch respectively. From our calculations of the vertical structure we obtain (see Ludwig et al. 1994)

$$\Sigma_{\rm A} = 32\,{\rm g\,cm^{-2}}\ {M_{\rm WD,1}}^{-0.37}\, r_{10}^{1.10}\, \alpha_{\rm h,0.2}^{-0.8}\, \mu_{0.6}^{0.75}, \quad (18)$$

$$\Sigma_{\rm B} = 185\,{\rm g\,cm^{-2}}\ {M_{\rm WD,1}}^{-0.37}\, r_{10}^{1.10}\, \alpha_{\rm c,0.05}^{-0.8}\, \mu_{1.0}^{0.4}, \quad (19)$$

$$T_{\rm eff,A} = 8322\,{\rm K}\ {M_{\rm WD,1}}^{0.03}\, r_{10}^{-0.1}, \quad (20)$$

$$T_{\rm eff,B} = 6317\,{\rm K}\ {M_{\rm WD,1}}^{0.03}\, r_{10}^{-0.1}, \quad (21)$$

where $\alpha_{\rm c,0.05} = \alpha_{\rm cool}/0.05$. For the mid-plane temperature at these points we get

$$T_{\rm A} = 35503\,{\rm K}\ \alpha_{\rm h,0.2}^{-0.2}\, {M_{\rm WD,1}}^{-0.014}\, r_{10}^{0.043}\, \mu_{0.6}^{0.25}, \quad (22)$$

$$T_{\rm B} = 13588\,{\rm K}\ \alpha_{\rm c,0.05}^{-0.2}\, {M_{\rm WD,1}}^{-0.01}\, r_{10}^{0.03}\, \mu_{1.0}^{0.6}. \quad (23)$$

Similar relations were obtained by Cannizzo (1993) and Ichikawa & Osaki (1992). The effective temperature for the unstable branch is approximated by the interpolation formula

$$\log T_{\rm eff} = \frac{\log(T/T_{\rm A})}{\log(T_{\rm B}/T_{\rm A})} \log\left(\frac{T_{\rm eff,B}}{T_{\rm eff,A}}\right) + \log T_{\rm eff,A}\,. \quad (24)$$

2.2.3. The cool optically thin branch

The cool branch includes optically thick structure for higher temperatures (see Sect. 2.2.4) and optically thin structure for low temperatures. For the cool optically thin branch we use the formula given by Ichikawa & Osaki (1992). For convenience we have defined an effective temperature for the optically thin state by setting the radiative flux F equal $\sigma T_{\rm eff}^4$. We get

$$T_{\rm eff} =$$

$$3416\,{\rm K}\ \left(\frac{T}{3416}\right)^{2.37} \left(\frac{\Sigma}{78}\right)^{0.41} {M_{\rm WD,1}}^{0.08}\, r_{10}^{-0.23}\, \mu_{1.24}^{0.08}. \quad (25)$$

2.2.4. The cool optically thick branch

This branch is approximated analoguously to the unstable intermediate branch. For the point T, which marks the transition from the cool optically thick to the cool optically thin state, we obtain with Eq. (25)

$$\Sigma_{\rm T} = 78\,{\rm g\,cm^{-2}}\ {M_{\rm WD,1}}^{-0.35}\, r_{10}^{1.07}\, \alpha_{\rm c,0.05}^{-0.53}\, \mu_{1.24}^{0.44}, \quad (26)$$

$$T_{\rm eff,T} = T_{\rm T} = 3416\,{\rm K}\ {M_{\rm WD,1}}^{0.05}\, r_{10}^{-0.15}\, \alpha_{\rm c,0.05}^{0.16}\, \mu_{1.24}^{-0.19}. \quad (27)$$

Dissociation of molecules and the resulting change of μ can lead, for some parameter combinations, to a negative slope of this branch. Such a disk structure is thermally and diffusively unstable. The effective temperature on the cool optically thick branch is given by interpolation between points B and T,

$$\log T_{\rm eff} = \frac{\log(T/T_{\rm B})}{\log(T_{\rm T}/T_{\rm B})} \log\left(\frac{T_{\rm eff,T}}{T_{\rm eff,B}}\right) + \log T_{\rm eff,B}\,. \quad (28)$$

With Eqs.17, 24, 25 and 28 the cooling function is completely defined.

2.3. The solution of the partial differential equations

The partial differential equations are solved by using the method of finite-differences with a time-explicit, multi-step solution procedure (see Stone & Norman 1992, Müller 1994). The accretion disk is divided into concentric rings of finite width, which are numbered from 1 to N. Number 1 is the innermost and number N the outermost ring. For the inner and outer boundary condition two "ghost-rings" with numbers 0 and N+1 are formally

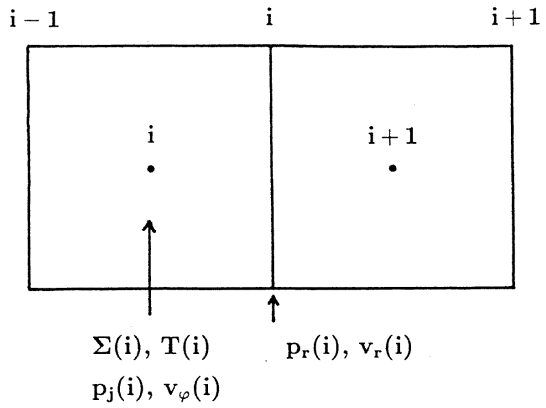

Fig. 1. Illustration of the discretisation of the one-dimensional computational domain.

added. Each concentric ring has an inner and outer boundary, which are numbered as follows. The inner boundary of the i-th ring with i-1, the outer boundary with i. The variables surface density, mid-plane temperature, and azimuthal velocity are assigned at the center of rings, while the radial flow velocity is assigned on the interfaces (for illustration see Fig. 1).

The radial coordinate of the center of the ring number 0 is equal to the radius of the white dwarf. At this inner boundary we assume $\Sigma = 0$ and $T = 0$. At the center of the rings number 0 and 1 the azimuthal velocity is taken as Keplerian. With Keplerian velocity the equation of angular momentum conservation yields:

$$\dot{M} = 3\pi \left(f + 2r \frac{\partial f}{\partial r} \right) . \tag{29}$$

This equation is used for calculating the radial momentum at the interface between the rings number 0 and 1. The outer boundary is treated similarly: at the center of the rings N and N+1 the azimuthal velocity is set equal to the Keplerian flow velocity. For the radial coordinate of the center of the ring N we take 70 percent of the primary's critical Roche radius $R_{1,\mathrm{R}}$. At the interface N a constant mass transfer rate $\dot{M}_{\mathrm{T}}$ is taken. The temperature at the center of the ghost-ring N+1 is the same as that of the ring N. This means that the temperature gradient at the interface N is zero. The assumption of Kepler velocity at the inner and outer boundary and the asumption of zero temperature gradient at the outer boundary are made for definitenes. Physical situations in real disks might differ from this. One expects, however, that this differences "gets lost" a few grid points away from the boundary.

As already mentioned, we use a two-alpha description as has been shown necessary to fit observed light curves in all computations for dwarf nova outbursts. Here, the alpha-value for each ring is defined in the following way:

$$\alpha = \alpha_{\mathrm{hot}} \quad \text{for } T_{\mathrm{eff}} \geq T_{\mathrm{eff,A}} ,$$

$$\alpha = \alpha_{\mathrm{cool}} \left(1 + \left[\frac{\alpha_{\mathrm{hot}}}{\alpha_{\mathrm{cool}}} - 1 \right] \frac{\log(T_{\mathrm{eff}}/T_{\mathrm{eff,B}})}{\log(T_{\mathrm{eff,A}}/T_{\mathrm{eff,B}})} \right)$$

$$\text{for } T_{\mathrm{eff,A}} > T_{\mathrm{eff}} > T_{\mathrm{eff,B}} ,$$

$$\alpha = \alpha_{\mathrm{cool}} \quad \text{for } T_{\mathrm{eff}} \leq T_{\mathrm{eff,B}} ,$$

where for our calculations we have set $\alpha_{\mathrm{hot}} = 0.2$ and $\alpha_{\mathrm{cool}} = 0.05$.

Since we use an explicit method for the time integration, the validity of the Courant-Friedrichs-Lewi-condition is checked at each time step in order to guarantee numerical stability.

3. Results

3.1. Initial distribution

We take as model parameters those of the system VW Hydri. The orbital parameters are (see Ritter & Kolb 1993): period P = 1.78 h, mass of the white dwarf $M_{\mathrm{WD}} = 0.63 M_{\odot}$, mass of the secondary $M_{\mathrm{Sec}} = 0.11 M_{\odot}$. For the outer disk boundary we take $R_{\mathrm{d}} = 1.7 \times 10^{10}$ cm (= 70% of primary's Roche radius). The disk's inner edge is set equal to the radius of the white dwarf $R_{\mathrm{i}} = 8.4 \times 10^{8}$ cm (determined from M_{WD} according to Nauenberg 1972). For the mass inflow rate at the outer radius we take a value derived from observations: $\dot{M}_{\mathrm{T}} = 5 \times 10^{15}$ g s^{-1} (Cannizzo et al. 1988). The total number of mesh points used in this calculation is 200. This is enough to resolve the detailed structure of transition fronts as confirmed by test calculations with 500 grid points. Cannizzo (1993) also had found that at least 100 grid points are necessary.

We start our computations of the outburst cycles with a stationary hot mass distribution. With arbitrary initial distribution of Σ, the stationary state is obtained by taking $\dot{M}_{\mathrm{T}}$ a factor 100 times higher than the observed value. This rate is higher than the critical rate $\dot{M}_{\mathrm{A}}(R_{\mathrm{d}})$ at the outer disk boundary below which dwarf nova behavior would set in. Once the stationary state is numerically established, we lower $\dot{M}_{\mathrm{T}}$ to the observed value and start a long-term calculation of the accretion disk.

Our code generates a strictly regular outburst behavior: two short outbursts alternate with one long outburst. In the following we describe the results for the outburst cycles starting with the onset of a long outburst.

3.2. Rise to a long outburst

First we show results for the change to the hot state. Figs. 2, 3 and 4 show the evolution of $\Sigma, T, T_{\mathrm{eff}}$ and v_{r} during the onset of a long outburst. An outward propagating heating wave, which has started near the inner disk edge, transforms the entire disk into the hot state. It is interesting to see in Fig. 2, that a narrow spike in Σ builts up at the heating front. The peak of the spike does not exceed the upper critical line Σ_{B}. Through radial energy flux carried by viscous processes, the critical temperature inside the heating wave is exceeded although Σ stays below the critical surface density Σ_{B}.

The double peaked Σ distribution in the heating wave arises if the material on the cool side of the front is optically thin. In

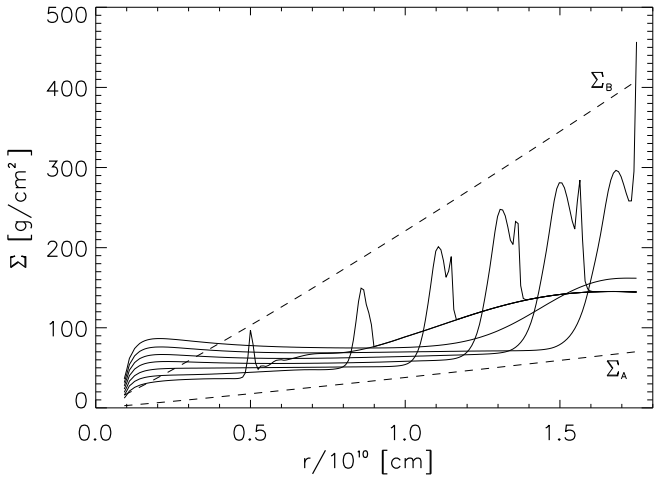

Fig. 2. The evolution of the surface density with time when a heating wave propagates outward. The dashed lines give values $\Sigma_{\rm A}$ and $\Sigma_{\rm B}$.

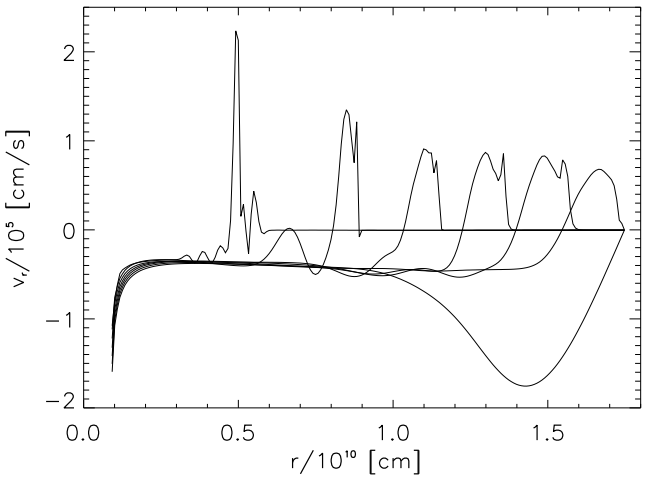

Fig. 4. The evolution of the radial flow velocity with time when a heating wave propagates outward.

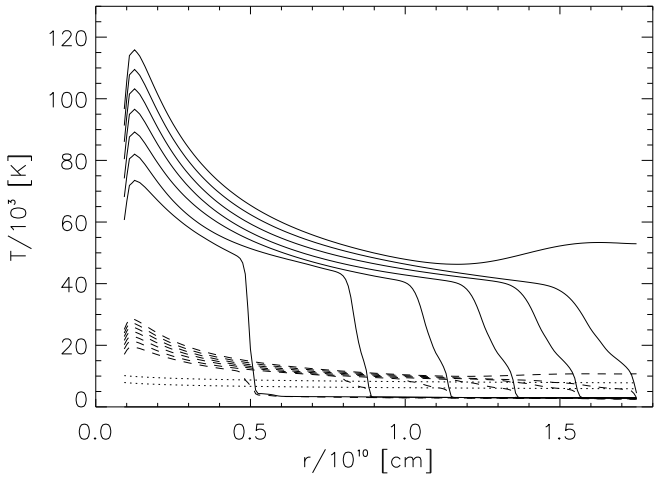

Fig. 3. The evolution of the temperature with time when a heating wave propagates outward. Solid lines show the midplane temperature distribution, dashed lines the effective temperature distribution (increase of temperature with time). The dotted lines give values $T_{\rm eff,A}$ (upper line) and $T_{\rm eff,B}$ (lower line).

the transition to the hot state two unstable regimes of the f - Σ - relation are involved: the unstable intermediate branch, producing the first maximum, and an unstable part of the cool optically thick branch (compare Sect. 2.2.4), producing the second maximum. The latter effect is due to dissociation of molecules on the transition from an optically thin to an optically thick cool state. Dissociation leads to an unstable regime of the equilibrium f - Σ -relation: in the lower part of the cool optically thick branch there is $\partial f/\partial\Sigma < 0$. This part of the branch is, like the unstable intermidiate branch, thermally and diffusively unstable.

We further see, that the surface density on the hot side of the front is lower than on the cool side. We will later see (Sect. 3.5), that this is especially important for short outbursts, where heating waves are reflected as cooling waves before the entire disk is transformed to the hot state.

Fig. 3 shows the evolution of the temperature distribution. In that part of the disk, which has been transformed to the hot state, the temperature distribution is similar to that of a hot stationary disk. We see the high temperature region expanding to the outer disk for the consecutive time steps. The steep decrease marks the border of the hot structure.

When the heating wave reaches the outer boundary, all the material interior to the heating wave has been transformed to the hot state. For a short time after the transition this leads to relatively high temperatures and high inward directed radial flow velocities in the outer region of the disk (see Fig. 4). In each of the Figs. 2, 3 and 4 this distribution of the corresponding quantity is shown at a time shortly after the entire disk was transformed to the hot state as the last of the 7 consecutive states.

As for the surface density, a narrow spike in the $v_{\rm r}$ distribution is characteristic for the heating wave regime. One notes that, for the entire hot part of the disk, the radial flow velocity is directed inward. This is possible because the heating wave is able to store mass and angular momentum.

In addition to the main results for disk evolution in Figs. 2, 3 and 4 we show in Fig. 5 the azimuthal velocity v_φ relative to the Kepler velocity $v_{\varphi,\rm K}$. We see, that even inside the heating wave, the deviation from the Keplerian value is only a few percent. The gradient of Ω relative to the Keplerian gradient $\partial\Omega_{\rm K}/\partial r$ is shown in Fig. 6, since this is the quantity relevant for the transition fronts. Inside the regime of the heating wave deviations up to $\sim$20% from the Keplerian value can occur. However, a test calculation, where we have assumed the disk to be Keplerian, has shown that these deviations, though they affect the detailed transition front structure, do not lead to a significant change of the outburst behavior. Thus it may be stated that deviations from Keplerian flow velocity lead only to small effects on the outburst behavior.

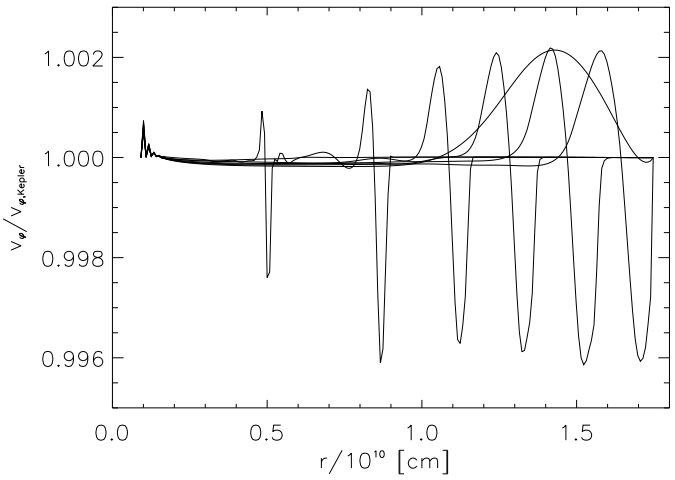

Fig. 5. The run of velocity v_φ relative to the Keplerian value when a heating wave propagates outward.

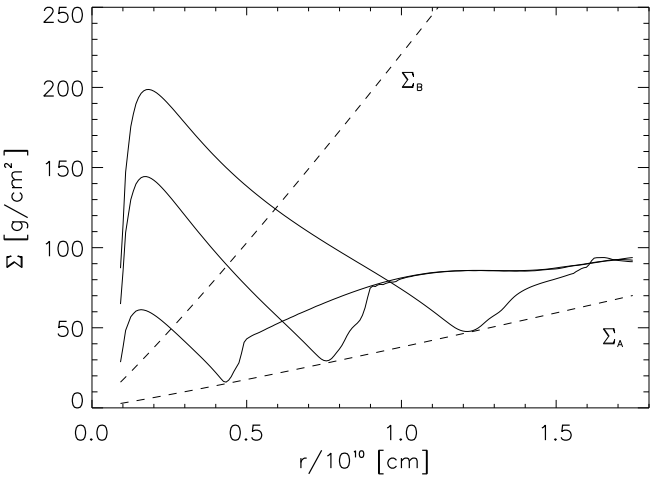

Fig. 7. The evolution of the surface density with time when a cooling wave propagates inward (Σ in the inner disk decreasing, in the outer disk approaching a distribution, which practically does not change during the time the disk changes to the cool state).

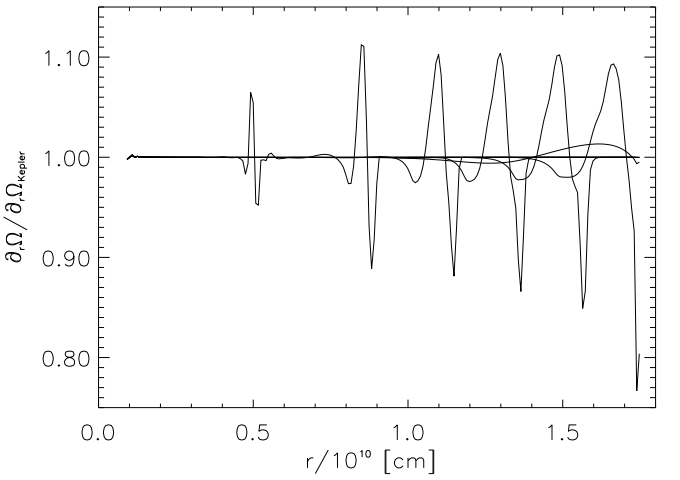

Fig. 6. The run of the gradient of Ω relative to the Keplerian value when a heating wave propagates outward.

3.3. Outburst maximum

Soon, after the entire disk is transformed into the hot state, a quasi-stationary state is established. In this state the surface density decreases in a self-similar way. This quasi-stationary state ends, as soon as the critical temperature $T_{\rm eff,A}$ is reached at the outer disk rim. A cooling wave starts to develop, which transforms the entire disk back to the cool state.

3.4. Decline from outburst

The evolution of the basic quantities Σ, T, $T_{\rm eff}$ and $v_{\rm r}$ is shown for three successive moments during the inward propagation of the cooling wave in Fig. 7, 8 and 9.

The Σ-distribution of the cooling wave (see Fig. 7) shows the following features: the front starts at the hot side with the value $\Sigma = \Sigma_{\rm A}$. One notes, that the value of the surface density never decreases below this value $\Sigma_{\rm A}$. Then Σ increases steeply inside the front, and finally turns into the relatively flat Σ-distribution of the cool disk. During the inward propagation of the cooliung wave the decrease of Σ is essential in the inner disk. The extend of the hot region from the inner edge to the location of the transition front ($\Sigma = \Sigma_{\rm A}$), becomes smaller and smaller. Further out Σ stays practically at the same value during this phase. The temperature decrease during this evolution is shown in Fig. 8.

At the hot side of the front ($\Sigma = \Sigma_{\rm A}$), the outward directed radial flow velocity reaches a maxima (see Fig. 9). It is interesting to note that for a wide range interior to the inward propagating cooling wave the mass flow is directed outwards (positive values of the flow velocity). While in the cool part of the disk nearly no transport of angular momentum occurs, it is an essential process in the hot part. At the hot side of the front the value of $v_{\rm r}$ decreases to the flow velocity (now directed again inward) of a cool disk. The radial flow velocities of a cool disk are two orders of magnitude smaller than those of the hot disk.

In Fig. 10 and 11 the corresponding deviations of v_φ and of $\frac{\partial\Omega}{\partial r}$ from the Kepler values are shown. They remain small through the whole cooling wave. On the formation of the cooling wave sound waves are generated at the outer disk boundary. Their damping is caused by the τ_{rr} and $\tau_{\phi\phi}$ components of the viscous stress tensor. At the beginning of the cooling phase, these sound waves cause additional deviations from the Keplerian flow velocity. However, also these deviations are small and can be neglected.

3.5. Rise to a short outburst

As mentioned already the resulting outbursts are alternatingly long and short. In the following we discuss the differences. Fig. 12 shows the evolution of the surface density with time during the heating phase for a short outburst. The important phenomenon is that the outward moving heating wave can not propagate to the outer disk edge. Instead the outward moving

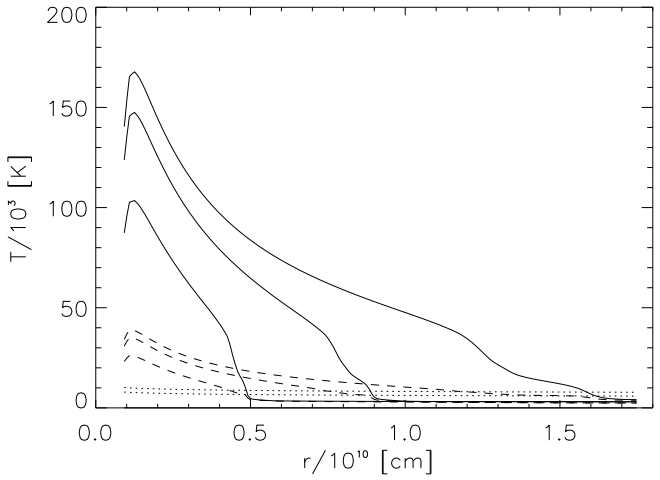

Fig. 8. The evolution of the temperature with time when a cooling wave propagates inward. The solid lines shows the central temperature, the dashed lines the effective temperature. The dotted lines give values $T_{\rm eff,A}$ (upper line) and $T_{\rm eff,B}$ (lower line).

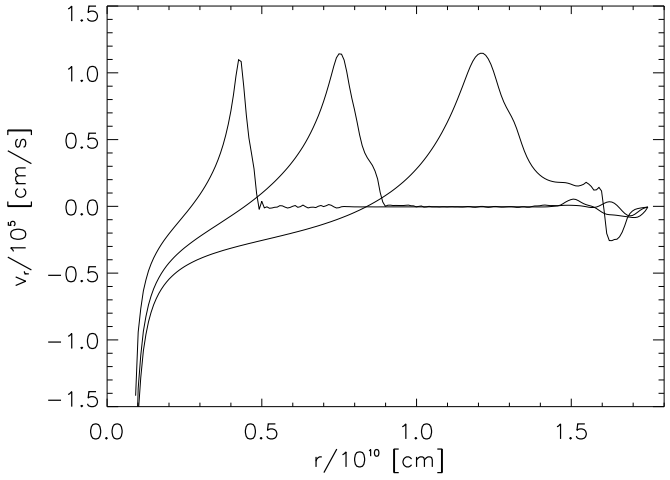

Fig. 9. The evolution of the radial flow velocity with time when a cooling wave propagates inward.

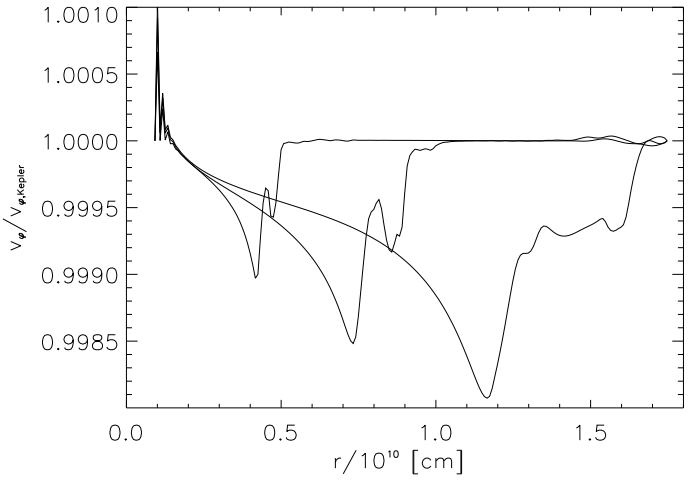

Fig. 10. Velocity v_φ in the disk relative to the Keplerian value when a cooling wave propagates inward.

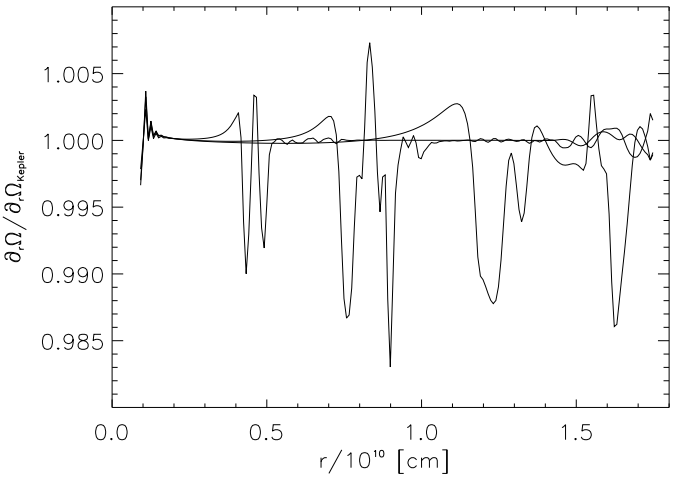

Fig. 11. The gradient of Ω relative to the Keplerian value when a cooling wave propagates inward.

heating wave is reflected as a cooling wave before it can reach the outer disk. The reflection occures, when the surface density on the hot side of the front has decreased to the value $\Sigma_{\rm A}$. No hot state is possible for $\Sigma < \Sigma_{\rm A}$. The subsequent evolution, i.e. the cooling phase, is shown in Fig. 13. So the essential difference between this evolution and that in a long outburst, where the heating wave reaches the outer disk edge, is the fact that the outer part of the disk remaines in the cool state.

In Fig. 14 the velocity $v_{\rm F}$ of the propagation of the instability during the short outburst is shown. The part of the curve with positive values of $v_{\rm F}$ shows the heating wave velocity, the part with negative values the cooling wave velocity. We obtain values for the transition front velocities which are comparable to those obtained by other authors (e.g. Meyer 1984, Mineshige 1987, Cannizzo 1993, Ludwig et al. 1994).

3.6. Long-term behavior

The long-term behavior of the accretion disk is shown in Fig. 15. Shown, from top to bottom, is the evolution of the visual luminosity, mass, and angular momentum of the disk, and the rate of mass accretion onto the central white dwarf. The visual luminosity of optically thin parts of the disk is set to zero. Parts of the quiescence, where the entire disk is in the optically thin state, shows up as gaps in the light curve. The small variations of the luminosity during the quiescence are caused by "tiny" transition waves running through a very small disk region. They are caused by the unstable part of the cool optically thick branch of the f - Σ -relation (compare Sect. 2.2.4).

The light curve shows the two types of outbursts, long ones and short ones. The two types results from differences in the

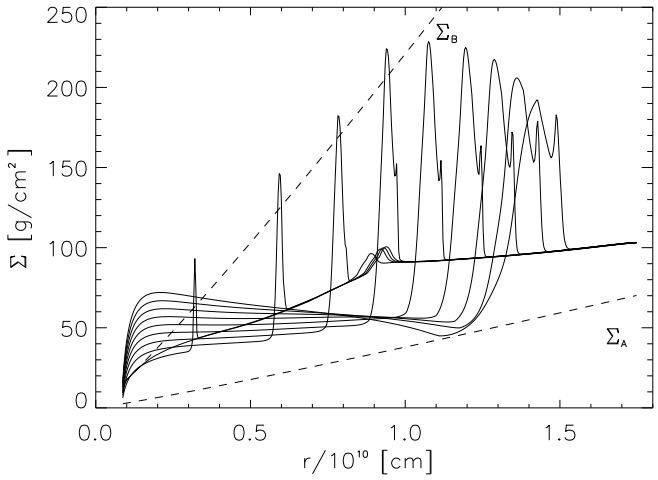

Fig. 12. The evolution of the surface density with time when a heating wave propagates outward in the case of a short outburst. Before the heating wave can reach the outer disk rim the wave is reflected as a cooling wave. The subsequent evolution is shown in Fig. 13.

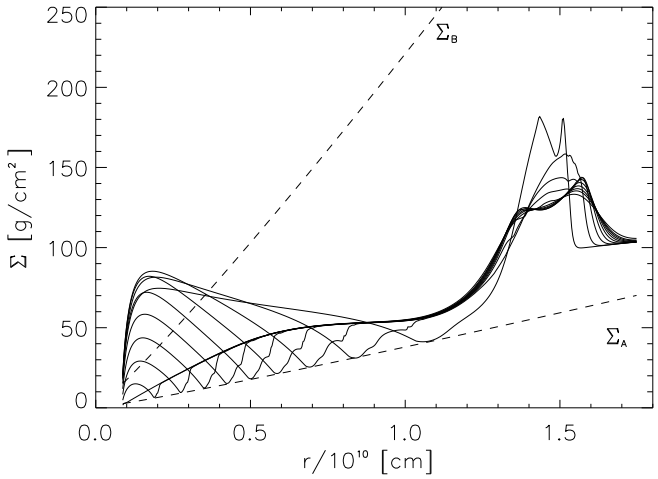

Fig. 13. The evolution of the surface density with time after the reflection of a heating wave as a cooling wave.

surface density distribution at the time of onset of the instability. For both types of outbursts, the instability starts near the inner edge of the disk. For outbursts which end up being long, the entire disk is transformed to the hot state. During such long outbursts about 30% of the disk mass and angular momentum are drained from the disk, mostly during the quasi-stationary hot state. Short outbursts result when the heating wave is not able to transform the entire disk to the hot state because the critical surface density $\Sigma = \Sigma_{\rm A}$ is reached on the hot side of the front before the front reaches the disk's outer edge. In such a case during the entire outburst, the outer part of the disk remains cool, and the disk loses less then 5% of its mass and angular momentum.

Our calculations show, that by an outward moving heating wave, mass is partially redistributed from inner parts to outer

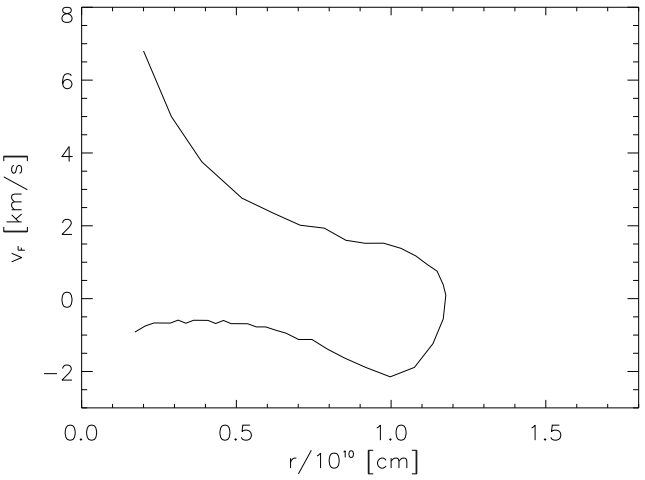

Fig. 14. The velocity $v_{\rm F}$ of the propagation of the instability. The part of the curve with positive values of $v_{\rm F}$ shows the heating wave velocity, the other part the cooling wave velocity.

parts of the disk. Thus, from short outburst to short outburst, the surface density in the outer part of the disk increases by both, the redistribution of mass by a heating wave and the mass transfer from the secondary. If finally after a sufficient number of short outbursts (here two), the surface density is high enough in the entire disk, the outward moving heating wave transforms the entire disk to the hot state. With this long outburst then a significant depletion occurs, so that the next two outburst are short again.

How many short outbursts lie between two long ones depends on the values of following parameters: the outer disk radius $R_{\rm d}$, the inner disk radius $R_{\rm i}$, the mass transfer rate $\dot{M}_{\rm T}$, the viscosity parameters $\alpha_{\rm hot}$ and $\alpha_{\rm cool}$, as investigated by Cannizzo (1993).

4. Discussion

4.1. The relevance of the terms in the energy equation

We have investigated the dependence of the outburst behavior on terms appearing in the energy equation similar to Cannizzo (1993). For this we have turned off different terms to judge from the resulting changes their importance.

From our calculations we have found, that lateral heat diffusion can be neglected outside of the transition front. Lateral heat diffusion is also unimportant in a cooling wave. However, the situation is different inside a heating wave. The radial energy flux carried by viscous diffusion leads to a significant broadening of the radial extension of the front. Further more we find that the radial energy flux carried by radiative diffusion can be neglected everywhere. Fig. 16 shows the evolution of the surface density during the outward propagation of a heating wave calculated without the lateral heat diffusion terms in the energy equation. If we compare this evolution with the one shown in Fig. 2 we see, that by turning off the lateral heat diffusion the heating wave becomes much narrower. The peak of the spike

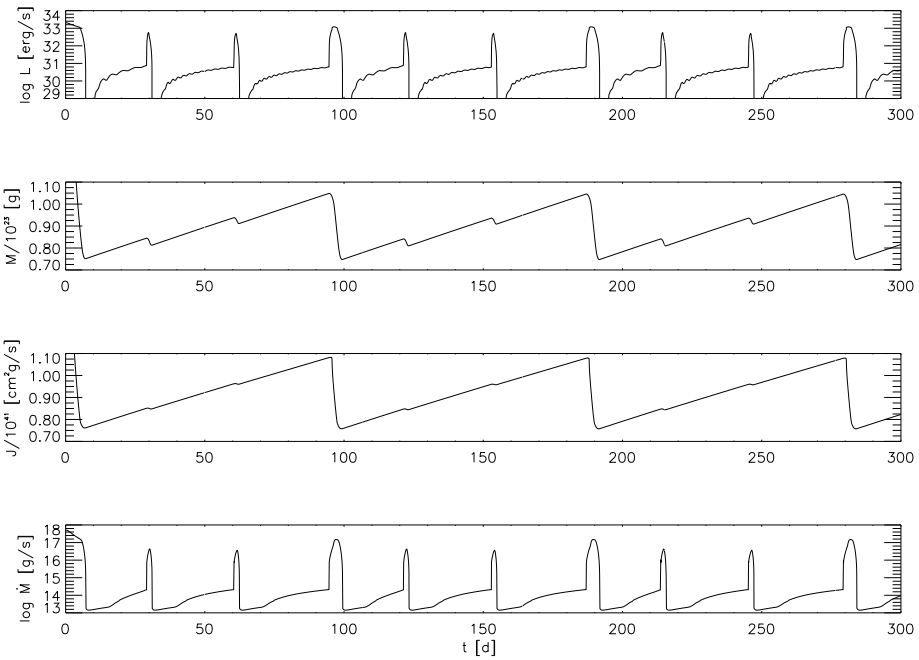

Fig. 15. Long term evolution of the accretion disk for parameters appropriate for VW Hyi. From top to bottom: the visual luminosity, the mass, and the angular momentum of the disk, and the mass accretion rate onto the central white dwarf as functions of time.

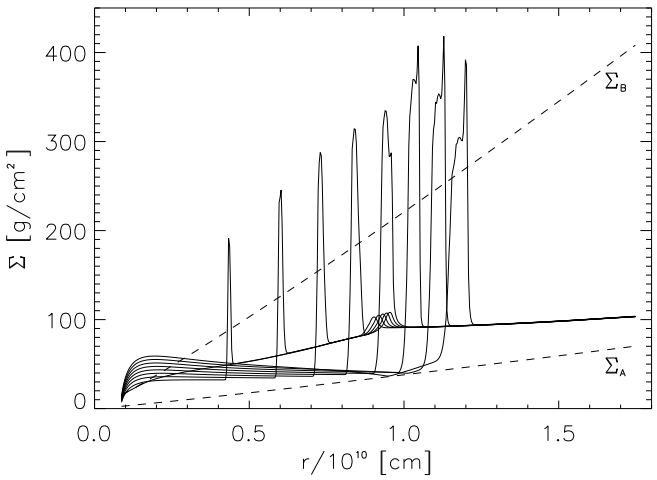

Fig. 16. The evolution of the surface density with time during the outward propagation of a heating wave. This calculation was carried out omitting the lateral heat diffusion terms in the energy equation, otherwise the same as Fig. 2.

of the heating wave exceeds the upper critical surface density $\Sigma_{\rm B}$. The resulting differences in the distribution of Σ inside the heating wave lead to a different redistribution of the mass inside the disk. Test calculations have shown, that the long-term behavior of a disk calculated without lateral heat diffusion is quite different from that calculated including it.

Neglecting the pressure term $2HT\left(\frac{\partial P}{\partial T}\right)_\rho \frac{1}{r}\frac{\partial}{\partial r}(rv_r)$ leads to only very small changes. The contribution of the frictional stresses τ_{rr} and $\tau_{\varphi\varphi}$ to the viscous heating is small compared to that of $\tau_{r\varphi}$ as expected. Even inside a heating wave, these contributions are three orders of magnitude smaller than the contribution from $\tau_{r\varphi}$. Nevertheless, these terms can not be neglected (in Eqs. 4 and 10) because they are responsible for the damping of sound waves. The advective term $C_{\rm V}\frac{1}{r}\frac{\partial}{\partial r}(rv_r\Sigma T)$ should not be neglected in calculation of dwarf nova outbursts, its neglect would make the width of the heating wave much smaller compared to that obtained including this term. Thus, the long-term behavior of the disk is strongly affected by the advective term.

4.2. The outburst pattern

The long-term light curve of SS Cyg, which includes observations since 1896 (see Cannizzo & Mattei 1992), shows a strong tendency for a bimodal outburst behavior. The alternation between one short and one long outburst is the most common behavior. The next most frequent behavior consists of stretches during which two short outbursts lie between two long ones. This behavior is reproduced in our calculations (see Fig. 15). The long outbursts are those in which the entire disk is transformed to the hot state, while in the short outbursts the outward moving heating wave is reflected as a cooling wave. A similar explanation is given by Cannizzo (1993). In our calculations both kinds of outburst start near the inner disk edge. This is a direct consequence of the two-alpha description used for the viscosity, where the parameters $\alpha_{\rm hot}$ and $\alpha_{\rm cool}$ are chosen to fit the durations of outburst and quiescence. But from observations of SS Cygni we know (see Mauche 1996), that at least the long outbursts can start near the inner disk edge (inside-out outbursts) as well as near the outer disk edge (outside-in outbursts). Within the two-alpha description outside-in outbursts can not be obtained by allowing for example small variations of the mass-transfer rate or by taking slightly different disk radii. What one needs for getting outside-in outbursts is a viscosity descriptions which produces a steep radial gradient in viscosity. This, for example, can be achieved by taking α proportional to

$(r/r_{\rm tidal})^x$ with $x > 0$, where $r_{\rm tidal}$ is the tidal radius which is about $1/3$ of the binary separation. Ichikawa & Osaki (1992) used such an α parametrization to obtain an outside-in outburst. Also an (H/r)-dependent α can lead to outside-in outbursts (Meyer & Meyer-Hofmeister 1984). For the modeling of the system SS Cyg one needs a viscosity description which allows both inside-out and outside-in outbursts. For the multi-modal outburst behavior this would mean that a long outburst can start from either edge of the disk. For example, it could be possible that due to small variations in the mass-transfer rate from the secondary sometimes the critical surface density for the long outburst is first reached in the inner disk region sometimes first in the outer region. However, within the framework of this model short outbursts cannot start at the outer edge.

4.3. The superoutburst phenomenon

Finally, in this section we show a connection to the superoutburst phenomenon of SU UMa stars. Three different models have so far been proposed to explain this phenomenon (for a review see Osaki 1996): (1) the enhanced mass-transfer model, (2) the thermal limit-cycle model, and (3) the thermal-tidal instability model. Here, we consider in particular the second model. In this model the superoutburst and the normal outburst of SU UMa stars are identical to the long and short outbursts seen in dwarf novae above the period gap (van Paradijs 1983). Howell et al. (1995) adopted this model arguing that the thermal limit-cycle instability is complex enough to produce several short outbursts sandwiched between two successive long outbursts. The supercycle of SU UMa stars would then be understood just by the thermal limit-cycle instability model of dwarf novae. Our calculations show (see Fig. 15), that indeed a supercycle light curve of SU UMa stars (here VW Hydri) can be produced with only the thermal limit-cycle instability operating inside the disk. The "superhump" phenomenon observed after the superoutburst has begun and which is explained by the 3:1 resonance between Kepler frequency at the outer disk and orbital frequency would then be a later consequence as the outbursting disk expands to the resonance radius, and not the cause for the superoutburst.

We note however, that observationally the superoutburst light curve seems to merge to a variable degree with the light curve of a preceding standart short outburst (Marino & Walker 1979, Warner 1995). The apparent variable superposition of the two light curves might indicate that the preceding short outburst does not directly trigger the superoutburst and might even have occasionally decayed significantly before the superoutburst takes its course. This would probably mean that the superoutburst occurs as an outward-in event whose beginning is not directly affected by the interior short outburst.

It will require further numerical investigation to see whether this course of events does require a release of the superoutburst by the 3:1 resonance as suggested by the Osaki model, or whether the phenomenon of alternating short and long outbursts will cover this case.

5. Comparison with other investigations

5.1. Computations by Mineshige

Mineshige (1987) has carried out fine mesh calculations which can almost fully resolve the transition fronts. He has found that the effects of lateral heat diffusion become very important only when the heating wave passes by. This is in full agreement with our results. From his results Mineshige concluded that lateral heat diffusion may modify more or less the transition wave propagation, but that drastic changes cannot be expected. From our calculations however, we have found that lateral heat diffusion leads to drastic changes of the long-term behavior of the disk. Regarding this point one has to note, that Mineshige used a somewhat different cooling function, which may of course influence the results. The main difference to his results concerns the profile of the heating wave. In his heating waves the peak of the spike exceeds the upper critical line $\Sigma_{\rm B}$. Also the width of the heating waves in his calculations is clearly smaller than in our calculations. Nevertheless, most of his results are qualitatively in good agreement with ours:
(1) The surface density distribution of a heating wave shows a profile with sharp spikes.
(2) The cooling wave starts on the hot side with the value $\Sigma = \Sigma_{\rm A}$. The value of Σ at each point does never drop below $\Sigma_{\rm A}$.
(3) The Σ distribution around the transition waves (Fig. 2, 7, 12 and 13) propagating in the disk are almost the same in both computations. The shape of the heating front is different from that of the cooling front.

Mineshige also discussed the localized front approximation. He concluded that the localized front approximation is relatively good for heating waves but it is marginal for cooling waves. This conclusion was drawn from the fact that only the width of a heating front is very small compared to its distance from the white dwarf, the width of a cooling wave is not. The validity of the localized front approximation will be discussed further down.

5.2. Computations by Cannizzo

Cannizzo (1993) examined how secular changes in the input parameters of the model affect the outbursts. He also examined the dependence of the outburst behavior on terms in the energy equation. His results agree with our present analysis:
(1) The advective term strongly influences the outburst behavior and is thus important.
(2) The pressure term can be neglected.
(3) The radial heat flux is only important in the region of a heating wave.
In his calculations Cannizzo considered only the radial energy flux due to viscous diffusion. The radial energy flux due to radiative diffusion was neglected because of numerical problems. But he notes, that from test calculations he has found the two terms to be comparable in magnitude. We have found here that only the radial energy flux due to viscous diffusion need be considered, the other flux can be neglected.

His results for cooling and heating waves and our results are qualitatively in good agreement. A noticeable difference however, concerns the maximum value of Σ inside a heating wave. In Cannizzo's calculations the spike of the heating wave is always close to the $\Sigma_{\rm B}$-line (see Fig. 3 in his paper).

Cannizzo's and our findings concerning a multi-modal outburst behavior are the same: The sequence of alternating long outbursts separated by one or several short outbursts is a natural consequence of the model. The mass present in the disk at the onset of the instability determines whether an outburst will be long or short. Cannizzo also notes, that the observed sequencing in the SU UMa systems can be explained in a natural way by the thermal instability alone and that the fact that the number of short outburst between two long outbursts is larger for systems below the period gap could be a consequence of the lower mass transfer rates in the SU UMa systems.

Another (at least ocassionally) observed feature in outbursts of SU UMa systems is that the recurrence time increases during the sequence of short normal outbursts between two superoutbursts. In Cannizzo's calculations such an outburst behavior was not obtained. In our calculations however, we find indeed such an increase of the quiescence between two short outbursts within the supercycle.

5.3. Earlier computations by Ludwig et al. (1994)

Finally, we compare our new calculations with our earlier work (Ludwig et al. 1994). In that paper results for simulations of VW Hydri, U Gem and SS Cygni were shown. For the simulations we used the localized front approximation (see Meyer 1984) for which the computing time required is only about 1% of that required here. The front velocities obtained in the present investigation are in good agreement with those obtained earlier. In particular, this agreement holds also for cooling wave velocities, despite the fact that the width of our cooling fronts are relatively broad. But, if one compares the calculated long-term evolution of the accretion disk in the simulation for VW Hydri, strong differences can be seen. Fig. 11 of Ludwig et al. (1994) shows the calculated light curve for VW Hydri: the outbursts repeat strongly periodically. This is a direct consequence of the boundary condition used at the front: it was assumed that Σ is the same on both sides of the front. By this, the outward moving heating wave has always transformed the entire disk into the hot state. A reflection of a heating wave as a cooling wave was not possible. In addition, the localized front approximation does not yield the redistribution of mass by a heating wave which is, however, very important for obtaining a multi-modal outburst behavior. Also the development of a transition front and the effects of lateral heat diffusion (broadening of a heating wave) are neglected within the localized front approximation.

Thus, for the detailed structure of transition waves and its consequences for the long-term behavior it is necessary to solve the diffusive evolution and the thermal adjustment simultaneously.

6. Conclusions

We have investigated outbursts in dwarf nova accretion disks in the framework of the disk instability model. The long-term evolution of an accretion disk was calculated with the high resolution required to resolve transition fronts adequately.

By solving the Navier-Stokes equations for the radial flow velocity and the azimuthal velocity we were able to take into account deviations of the azimuthal velocity from the Keplerian velocity. Though even inside a heating wave, the deviation from the Keplerian value is only a few percent, the gradient $\frac{\partial\Omega}{\partial r}$ can deviate byup to $\sim$20% from the Keplerian value influencing the distribution of heating and diffusion of angular momentum within the front. It turns out however, that this has only a small effects on the overall outburst behavior of the accretion disk.

A discussion of the energy equation reveales the following results: lateral heat diffusion is only important in the region of a heating wave. It leads to a considerable broadening of the wave. For this, only the radial energy flux carried by viscous processes is responsible, the radial energy flux carried by radiative processes can be neglected. While the pressure term $2HT\left(\frac{\partial P}{\partial T}\right)_\rho \frac{1}{r}\frac{\partial}{\partial r}(rv_r)$ may be neglected the advective term $C_{\rm V}\frac{1}{r}\frac{\partial}{\partial r}(rv_r\Sigma T)$ should not. The contribution of the frictional stresses τ_{rr} and $\tau_{\varphi\varphi}$ to the viscous heating is small compared to the contribution of $\tau_{r\varphi}$. Nevertheless, when compressibility is included these terms should not be neglected because they are responsible for the damping of sound waves.

A comparison with calculations by Mineshige (1987) and Cannizzo (1993) has shown general agreement with our results. Especially, our solutions show the multi-modal outburst behavior which was also obtained by Cannizzo. The underlying property for this is that long outbursts are those in which the entire disk is transformed to the hot state, while in short ones the outward moving heating wave is reflected as a cooling wave before reaching the outer disk rim. In our calculations all outbursts start near the inner disk edge. From observations of SS Cygni we know (see Mauche 1996), that at least long outbursts can start also near the outer disk edge. Within the usual two-alpha description for the viscosity such outside-in outbursts can not be obtained. For getting outside-in outbursts a viscosity prescription is needed which produces a sufficiently steep radial gradient of the viscosity. This, for example, can be achieved by taking α proportional to $(r/r_{\rm tidal})^x$ with $x > 0$, where $r_{\rm tidal}$ is the tidal radius which is about $1/3$ of the binary separation (see Ichikawa & Osaki, 1992). Also an (H/r)-dependent α can lead to outside-in outbursts (Meyer & Meyer-Hofmeister 1984). Alternatively, hole formation e.g. by disk evaporation during quiescence (Liu et al. 1997) may shift the point of triggering of the outburst outward.

Comparison of the present calculations with those by Ludwig et al. (1994) show that front velocities were obtained which are in good agreement with those obtained here. However, the localized front approximation in its simple form does not yield a complex (e.g. a bimodal) outburst behavior, since the detailed internal structure of transition waves decides on their formation

and fading with consequences for the long-term behavior of the disk.

Finally, our calculations have shown that within the thermal limit-cycle model of dwarf nova outbursts the observed sequencing in SU UMa systems can be explained in a natural way. Also the (at least occasionally) observed increase of the recurrence time during the sequence of short normal outbursts between two superoutbursts is succesfully obtained in our calculations.

Acknowledgements. The authors thank E. Meyer-Hofmeister and H. Ritter for critical reading of the manuscript and helpful discussions. We are also grateful to R. Stehle for kindly allowing us to use parts of his numerical code.

References

Bird R.B., Stewart W.E., Lightfoot E.N., 1966, Transport phenomena, Wiley, New York
Cannizzo J.K., 1993, ApJ 419, 318
Cannizzo J.K., Shafter A.W., Wheeler J.C.: 1988, ApJ 333, 227
Cannizzo J.K., Mattei J., 1992, ApJ 401, 642
Godon P., 1995, MNRAS 277, 157
Howell S.B., Szkody P., Cannizzo J.K., 1995, ApJ 439, 337
Ichikawa S., Osaki Y., 1992, PASJ 44, 15
Ichikawa S., Osaki Y.: 1994, PASJ, 46, 621
Liu B., Meyer F., Meyer-Hofmeister E., 1997, submitted to A&A
Ludwig K., Meyer-Hofmeister E., Ritter H., 1994, A&A 290, 473
Marino B.F., Walker, W.S.G., 1979. In: Bateson F.M., Smak J., Urch I.H. (eds.) Proc. IAU Coll. 46, Changing Trends in Variable Star Research, University of Waikato, Hamilton N.Z., p.29
Mason K.O., Cordova F.A., Watson M.G., King A.R., 1988, MNRAS 232, 779
Mauche C.W., 1996, in: Bowyer S., Malina R.F. (eds.) Astrophysics in the Extreme Ultraviolet, Kluwer, Dordrecht, p.317
Meyer F., 1984, A&A 131, 303
Meyer F., Meyer-Hofmeister E., 1984, A&A 132, 143
Meyer-Hofmeister, E., Ritter, H., 1993, Accretion Disks in Close Binaries. In: Sahade J., McCluskey G.E., Kondo Y. (eds.) The Realm of Interacting Binaries, Kluwer, Dordrecht, p.143
Mineshige S., 1987, ASS 130, 331
Mineshige S., Osaki Y., 1983, PASJ 35, 377
Müller E., 1994, Fundamentals of Gas-Dynamical Simulations. In: Contopoulos G., Spyrou N.K., Vlahos L. (eds.) Galactic Dynamics and N-body Simulations, Springer, Berlin, p.313
Nauenberg M., 1972, ApJ 175, 417
Novikov I.D., Thorne K.S., 1973, Black Hole Astrophysics. In: DeWitt C., DeWitt B.S. (eds.) Black Holes, Gordon & Breach, New York, p.343
Osaki Y., 1996, PASJ 108, 39
Ritter H., Kolb U., 1993, A compilation of cataclysmic binaries with known or suspected orbital periods. In: Lewin W.H.G., van Paradijs J., van den Heuvel E.P.J. (eds.) X-ray Binaries, Cambridge University Press, Cambridge, p.578 p.578–638
Shakura N.I., Sunyaev R.A., 1973, A&A 24, 337
Stone J.M., Norman M.L.C., 1992, APJ Suppl. 80, 753
Taam R.E., Lin D.N.C., 1984, APJ 287, 761
van Paradijs J., 1983, A&A 125, L16
Warner B., 1995, Cataclysmic Variable Stars. Cambridge Astrophysics Series 28, Cambridge University Press, Cambridge

This article was processed by the author using Springer-Verlag LaTeX A&A style file *L-AA* version 3.